Inorganic Chemistry
Article

Inorg. Chem. **2010**, *49*, 2969–2974 **2969**
DOI: 10.1021/ic9025014

Evaluation of [Ln(H_2cmp)(H_2O)] Metal Organic Framework Materials for Potential Application as Magnetic Resonance Imaging Contrast Agents

Giovannia A. Pereira,[†,‡] Joop A. Peters,[§] Filipe A. Almeida Paz,[‡] João Rocha,[‡] and Carlos F. G. C. Geraldes*[,†]

[†]*Department of Life Sciences, Faculty of Science and Technology, and Center of Neurosciences and Cell Biology, University of Coimbra, 3001-401 Coimbra, Portugal,* [‡]*Department of Chemistry, University of Aveiro, CICECO, 3810-193 Aveiro, Portugal, and* [§]*Laboratory of Biocatalysis and Organic Chemistry, Department of Biotechnology, Delft University of Technology, Julianalaan 136, 2628 BL Delft, The Netherlands*

Received December 16, 2009

Aqueous suspensions of metal organic frameworks (MOF) containing different Ln^{3+} ions, consisting of a series of layered Ln^{3+} networks formulated as [Ln(H_2cmp)(H_2O)] (where H_5cmp is (carboxymethyl)iminodi(methylphosphonic acid), with a relatively wide size distribution (400 nm to 1 μm) were studied by relaxometry. The water ^{1}H longitudinal (r_1) and transverse (r_2) relaxivities were obtained for aqueous suspensions of these materials with different lanthanide ions. The values of r_1 are very small and varied only slightly with the effective magnetic moment (μ_{eff}) of the lanthanide ions, while r_2 values are larger and proportional to the value of μ_{eff}^2. The dependence of R_2 on τ_{CP} (the time interval between two consecutive refocusing pulses in the train of 180° pulses applied in a CPMG pulse sequence) was evaluated. The value of R_2 initially increases with τ_{CP} and then saturates at higher τ_{CP} at a value that is about 3 to 5 times lower than R_{2p}*. This can be explained by the static dephasing regime (SDR) theory, in which the diffusion effect is taken into account and where the condition $\tau_D > \Delta\omega(r_p)^{-1}$ holds ($\tau_D = r_p^2/D$, where D is the diffusion coefficient, r_p is the radius of the particle, and $\Delta\omega(r_p)$ is the Larmor frequency shift at the particle's surface). Separation of the particles into two fractions with different particle sizes led to a significant enhancement of the r_2 relaxivity of the smaller particles with a narrow size distribution. Magnetometric measurements performed with the particles containing Dy(III), Ho(III), and Gd(III) showed a typical paramagnetic behavior from 4 to 100 K, used to determine the Curie constants.

Introduction

Molecular Imaging applications of Magnetic Resonance Imaging (MRI), despite the high spatial resolution (μm) of the technique, must overcome its low sensitivity.[1] Because of this limitation, the investigation of molecular events at the cellular level requires a relatively large local concentration of contrast agent (CA) reporting groups to achieve an observable contrast enhancement. The ideal targeted MRI CA should allow the detection of molecular events at the nanomolar concentration range. This is usually not feasible with targeted CAs containing as reporting group(s) one or even a small number of Gd^{3+} chelates per targeting group, which have limited efficiency in enhancing the water proton relaxation rates ($1/T_1$ and/or $1/T_2$), usually expressed as the longitudinal and transverse relaxivity values, r_1 and r_2, respectively (in s^{-1} per mM of Gd).[2a,b] Nanoparticulate CAs enable the delivery of a high payload (tens, hundreds, or even thousands) of paramagnetic ions reporters to each target site.[3−5]

Magnetic nanoparticles have a wide range of applications as CAs[6] and, depending on the r_2/r_1 ratios, they can be useful as CAs for T_2-weighted (negative contrast) and/or T_1-weighted (positive contrast) imaging. Their pharmacokinetics depends on the particle size,[7,8] and intravenous administration is only possible for particle sizes below the micrometer range. Larger particles, such as Gadolite, a Gd^{3+}-modified NaY zeolite,[9] are trapped in lung alveoli and can only be used for the examination of the gastrointestinal tract. Intermediate size particles are taken up by the reticulo- endothelial system of the liver and other organs, while particles smaller than 100 nm can be used to image lymph nodes.[10] Nanoparticles have been conjugated

*To whom correspondence should be addressed. E-mail: geraldes@bioq.uc.pt.

(1) Weissleder, R.; Mahmood, U. *Radiology* **2001**, *219*, 316–333.
(2) (a) Caravan, P.; Thomas, J. E.; McMurry, T. J.; Lauffer, R. B. *Chem. Rev*. **1999**, *99*, 2293–2352. (b) Tóth, É; Helm, L.; Merbach, A. *Top. Curr. Chem*. **2002**, *221*, 61–101.
(3) Aime, S.; Frullano, L.; Crich, S. G. *Angew. Chem., Int. Ed.* **2002**, *41*, 1017–1019.
(4) Sitharaman, B.; Kissell, K. R.; Hartman, K. B.; Tran, L. A.; Baikalov, A.; Rusakova, I.; Sun, Y.; Khant, H. A.; Ludtke, S. J.; Chiu, W.; Laus, S.; Toth, E.; Helm, L.; Merbach, A. E.; Wilson, L. *J. Chem. Commun.* (*Camb*) **2005**, 3915–3917.
(5) McDonald, M. A.; Watkin, K. L. *Acad. Radiol*. **2006**, *13*, 421–427.
(6) Muller R. N.; Roch A.; Colet J.-M.; Ouakssim A.; Gillis P. *The Chemistry of Contrast Agents in Medical Magnetic Resonance Imaging*; John Wiley & Sons,Ltd.: Chichester, 2001; pp 417−435.
(7) Weissleder, R.; Reimer, P. *Eur. Radiol*. **1993**, *3*, 198–212.
(8) Pankhurst, Q. A.; Connolly, J.; Jones, S. K.; Dobson, J. *J. Phys. D: Appl. Phys*. **2003**, *36*, R167–R181.
(9) Balkus Jr., K. J.; Sherry, A. D.; Young, S. W. U.S. Patent 5, 122, 363 A, **1992**.
(10) Reynolds, C. H.; Annan, N.; Beshah, K.; Huber, J. H.; Shaber, S. H.; Lenkinski, R. E.; Wortman, J. A. *J. Am. Chem. Soc*. **2000**, *122*, 8940–8945.

Published on Web 02/12/2010

with targeting groups. For example, perfluorocarbon Gd^{3+}-containing nanoparticles have been conjugated with antibodies to target a human thrombus,[11] or the $\alpha_V\beta_3$ integrin receptor in cancer angiogenesis.[12,13] Lanthanide oxides (in particular dysprosium and holmium oxide) are an interesting class of magnetic materials, which have been studied in terms of their transverse relaxivity properties at high magnetic field strengths.[14,15a] Luminescent hybrid nanoparticles with a paramagnetic gadolinium oxide core have been applied as bimodal CAs for in vivo optical and MR imaging.[15b] Finally, colloidal suspensions of superparamagnetic (SPM) particles have been extensively studied, and depending on their sizes and r_2/r_1 ratios, have found applications as CAs to obtain negative or positive contrast in T_2- or T_1-weighted images, respectively.[6,16−18]

The vast majority of nanosized imaging probes have purely inorganic materials, such as quantum dots, SPM metal oxides, and gold nanoparticles. Metal organic frameworks (MOFs) are a new class of crystalline hybrid materials consisting of metal ions or clusters coordinated to often rigid organic molecules to form one-, two-, or three-dimensional structures that can be porous, making them applicable in gas purification and separation,[19−25] catalysis,[26−29] and optical/magnetic sensors.[30−33] Furthermore, nanoscale MOFs have been proposed as a new class of imaging probes.[34]

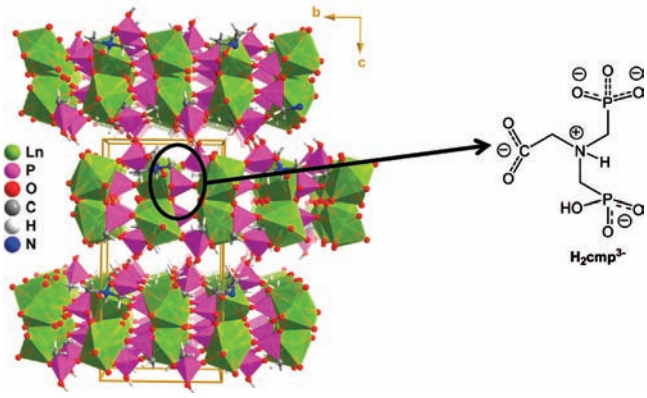

Figure 1. Perspective views of the crystalline structure of the [Ln(H2cmp)(H2O)] particles (left) and chemical drawing of the organic moiety (H_2cmp^{3-}) (right).

We have recently reported a series of new Ln^{3+}-containing hybrid materials consisting of a series of layered Ln^{3+} networks formulated as [Ln(H_2cmp)(H_2O)] (H_5cmp is (carboxymethyl)iminodi(methylphosphonic acid); Ln = La^{3+}, Pr^{3+}, Nd^{3+}, Sm^{3+}, Eu^{3+}, Gd^{3+}, Tb^{3+}, Dy^{3+}, Ho^{3+} and Er^{3+}).[35] The Ln^{3+} centers in these networks have a highly distorted dodecahedral coordination environment with one water molecule in the first coordination sphere (Figure 1). Noteworthy, in the polymeric structures the organic molecule H_5cmp undergoes proton transfer to originate H_2cmp^{3-} (Figure 1).These hybrid materials have been developed for potential applications in many different areas and for that, the photoluminescent and catalytic properties were extensively studied.[35] Some intrinsic characteristics of the [Ln(H_2cmp)(H_2O)] particles lead us to evaluate their potential as MRI CAs, such as (i) the presence of the lanthanide ions in the framework, contributing to the lower possibility of leaching of the toxic Ln^{3+} ion and (ii) the evidence for the presence of one water molecule in the inner coordination sphere of the Ln^{3+} ion. Thus, in this paper we describe a study on aqueous suspensions of these novel MOFs, namely, their size distribution and relaxometric properties, in particular the r_1, r_2* and r_2 relaxivities. The results obtained are compared with those recently reported for other Ln^{3+}-containing hybrid materials.[34a−c]

Experimental Section

Synthetic procedures and characterization of the [Ln(H_2cmp)(H_2O)] materials were described previously.[35] NMR measurements were carried out with aqueous suspensions of these materials, prepared by suspending a weighed amount of the concerning particles in a weighed amount of doubly distilled water followed by dispersion using an ultrasonic bath during 10 min. No leaching of lanthanide ions from the

(11) Yu, X.; Song, S. K.; Chen, J.; Scott, M. J.; Fuhrhop, R. J.; Hall, C. S.; Gaffney, P. J.; Wickline, S. A.; Lanza, G. M. *Magn. Reson. Chem.* **2000**, *44*, 867–872.
(12) Winter, P. M.; Morawski, A. M.; Caruthers, S. D.; Fuhrhop, R. W.; Zhang, H.; Williams, T. A.; Allen, J. S.; Lacy, E. K.; Robertson, J. D.; Lanza, G. M.; Wickline, S. A. *Circulation* **2003**, *108*, 2270–2274.
(13) Morawski, A. M.; Winter, P. M.; Crowder, K. C.; Caruthers, S. D.; Fuhrhop, R. W.; Scott, M. J.; Robertson, J. D.; Abendschein, D. R.; Lanza, G. M.; Wickline, S. A. *Magn. Reson. Chem.* **2004**, *51*, 480–486.
(14) Norek, M.; Pereira, G. A.; Geraldes, C. F. G. C.; Denkova, A.; Zhou, W.; Peters, J. A. *J. Phys. Chem. C.* **2007**, *111*, 10240–10246.
(15) (a) Norek, M.; Kampert, E.; Zeitler, U.; Peters, J. A. *J. Am. Chem. Soc.* **2008**, *130*, 5335–5340. (b) Bridot, J.-L.; Faure, A.-C.; Laurent, S.; Rivière, C.; Billotey, C.; Hiba, B.; Janier, M.; Josserand, V.; Coll, J.-L.; Vander Elst, L.; Muller, R. N.; Roux, S.; Perriat, P.; Tillement, O. *J. Am. Chem. Soc.* **2007**, *129*, 5076–5084.
(16) Groman, E. V., Josephson, L., Lewis, J. M. U.S. Patent 4827945, **1990**.
(17) Reimer, P.; Muller, M.; Marx, C.; Wiedermann, D.; Muller, R.; Rummeny, E. J.; Ebert, W.; Shamsi, K.; Peters, P. E. *Radiology* **1998**, *209*, 831–836.
(18) Weissleder, R.; Elizondo, G.; Wittenberg, J.; Rabito, C. A.; Bengele, H. H.; Josephson, L. *Radiology* **1990**, *175*, 489–493.
(19) Yaghi, O. M.; Li, G. M.; Li, H. L. *Nature* **1995**, *378*, 703–706.
(20) Dinca, M.; Han, W. S.; Liu, Y.; Dailly, A.; Brown, C. M.; Long, J. R. *Angew. Chem., Int. Ed.* **2007**, *46*, 1419–1422.
(21) Kim, H.; Samsonenko, D. G.; Yoon, M.; Yoon, J. W.; Hwang, Y. K.; Chang, J. S.; Kim, K. *Chem. Commun.* **2008**, 4697–4699.
(22) Eddaoudi, M.; Kim, J.; Rosi, V.; Vodak, D.; Wachter, J.; O'Keefe, M.; Yaghi, O. M. *Science* **2002**, *295*, 469–472.
(23) Loiseau, T.; Lecroq, L.; Volkringer, C.; Marrot, J.; Férey, G.; Haouas, M.; Taulelle, F.; Bourrelly, S.; Llewellyn, P. L.; Latroche, M. *J. Am. Chem. Soc.* **2006**, *128*, 10223–10230.
(24) Ramsahye, N. A.; Maurin, G.; Bourrelly, S.; Llewellyn, P.; Loiseau, T.; Férey, G. *Phys. Chem. Chem. Phys.* **2007**, *9*, 1059–1063.
(25) Rosi, N. L.; Eckert, J.; Eddaoudi, M.; Vodak, D. T.; Kim, J.; O'Keeffe, M.; Yaghi, O. M. *Science* **2003**, *300*, 1127–1129.
(26) Xiau, B.; Hou, H.; Fan, Y. *J. Organomet. Chem.* **2007**, *692*, 2014–2020.
(27) Qiu, L.-G.; Gu, L.-N.; Hu, G.; Zhang, L.-D. *J. Sol. State Chem.* **2009**, *182*, 502–508.
(28) Xamena, F. X. L.; Casanova, O.; Tailleur, R. G.; Garcia, H.; Corma, A. *J. Catal.* **2008**, *25*, 220–227.
(29) Bonnet, F.; Visseaux, M.; Pereira, A.; Bouver, F.; Barbier-Baudry, D. *Macromol. Rapid Commun.* **2004**, *25*, 873–877.
(30) Lin, J. G.; Xu, Y. Y.; Qiu, L.; Zang, S. Q.; Lu, C. S.; Duan, C. Y.; Li, Y. Z.; Gao, S.; Meng, Q. J. *Chem. Commun.* **2008**, 2659–2661.
(31) Zhao, B.; Cheng, P.; Dai, Y.; Cheng, C.; Liao-Zheng, D.; Yan, S. P.; Jiang, Z. H.; Wang, G. L. *Angew. Chem., Int. Ed.* **2003**, *42*, 934–936.
(32) Li, F. Y.; Xu, L.; Gao, G. G.; Fan, L. H.; Bi, B. *Eur. J. Inorg. Chem.* **2007**, 3405–3409.
(33) Dias, A. B. *Dalton Trans.* **2007**, 2229–2241.
(34) (a) Taylor, K. M. L.; Jin, A.; Lin, W. *Angew. Chem., Int. Ed.* **2008**, *47*, 7722–7725. (b) Rieter, W. J.; Taylor, K. M. L.; An, H.; Lin, W.; Lin, W. *J. Am. Chem. Soc.* **2006**, *128*, 9024–9025. (c) Nishiabu, R.; Hashimoto, N.; Cho, T.; Watabane, K.; Yasugana, T.; Endo, A.; Kaneko, K.; Niidome, T.; Murata, M.; Adaci, C.; Katayama, Y.; Hashizume, M.; Kimizuka, N. *J. Am. Chem. Soc.* **2009**, *131*, 2151–2158.
(35) Silva, L. C.; Lima, S.; Ananias, D.; Silva, P.; Mafra, L.; Carlos, L. D.; Pillinger, M.; Valente, A. A.; Paz, F. A. A.; Rocha, J. *J. Mater. Chem.* **2009**, *19*, 2618–2632.

particles (specifically for Gd^{3+}-containing particles) was detected in aqueous suspensions during at least 30 days at physiological pH by using the xylenol orange method.[36]

All the ^1H NMR experiments were carried out at 499.82 MHz (Varian Unity 500 spectrometer). The bulk magnetic susceptibility (BMS) shifts (Δ_{BMS}) of the particle suspensions were measured using the Evans method[37,38] to determine accurate concentrations of lanthanide ions. In this method, the BMS is determined from the frequency shift of the *tert*-butyl alcohol signal with respect to a diamagnetic sample (1% *tert*-butyl alcohol in D_2O), which is proportional to the concentration of the paramagnetic ion with accuracy of about 1%.[38] Water proton longitudinal relaxation times (T_1) were measured using the inversion recovery pulse sequence, while water proton transverse relaxation times (T_2) were measured using a Carr−Purcell−Meiboon−Gill (CPMG) pulse sequence. The time interval between two consecutive refocusing pulses (τ_{CP}) in the train of 180° pulses applied was varied between 0.05 and 10 ms. The values of T_2*, the transverse relaxation time in the presence local field inhomogeneities, were obtained from the spectral linewidths. All the experimental values of the relaxation rates were corrected for diamagnetic contributions using aqueous suspensions of the Y^{3+}-containing particles under the same conditions. The samples had a concentration of 0.32 mg particle/mL of water. Measurements of the line width as a function of the concentration (data not shown) demonstrated that the R_2* was linearly dependent on the concentration for the concentration range used in this study. The computer fittings of the R_2 ($1/T_2$) data were carried out with a homemade computer program using the Micromath Scientist version 2.0 (Salt Lake City, Utah, U.S.A.) software.

Dynamic Light Scattering (DLS) measurements were carried out with a Malvern ZetaSizer Nano ZS series equipment (Malvern, U.K.). Scanning and Transmission Electron Microscopy (SEM and TEM, respectively) were collected using a (i) Hitachi SU-70 field emission gun tungsten filament instruments working typically at 25 kV for SEM and (ii) JEOL-TEM 200 kV for TEM. Magnetic susceptibility measurements were performed by Dr. Soma Das at the University of Aveiro, with a Quantum Design MPMS5 SQUID (superconducting quantum interference device) magnetometer. The measurements were taken under an applied magnetic field 51 mT on heating from 4.5 K up to 300 K. The samples were previously cooled with the magnetic field applied from room temperature to 4.5 K. Theoretical fitting of the magnetic susceptibility data was carried out by Dr. Victor Amaral at the University of Aveiro.

Results and Discussion

The size distribution of the [Ln(H_2cmp)(H_2O)] particles differs slightly with the lanthanide ion used. As these particles appeared to be very beam sensitive, the respective TEM images were not easy to obtain. For [Eu(H_2cmp)(H_2O)] only TEM images of particles were obtained, showing a very broad size distribution. The SEM and TEM images of the [Ln(H_2cmp)(H_2O)] crystals (Figure 2) show that the particles are thin plates (about 60 nm thick) with length and width varying between 400 and more than 1000 nm.

Magnetometric measurements of the susceptibility of [Ln(H_2cmp)(H_2O)] particles (Ln = Gd, Ho, and Dy) as a function of temperature (from 4 to 100 K) exhibit a simple

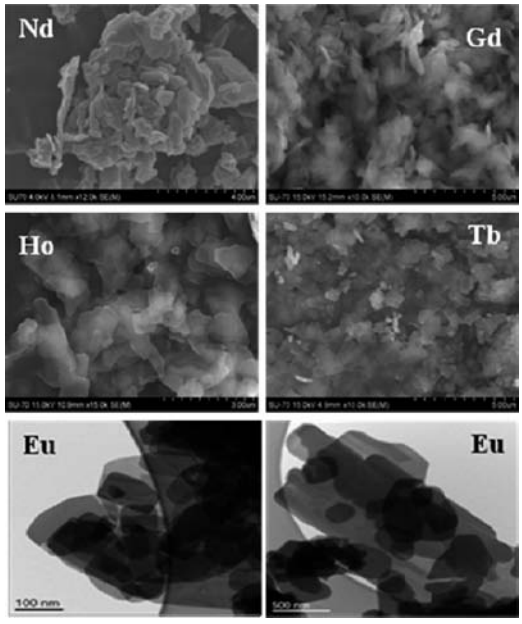

Figure 2. SEM images of [Ln(H_2cmp)(H_2O)] (Ln = Nd, Gd, Ho, Tb) (top four) and TEM images of [Eu(H_2cmp)(H_2O)] samples (bottom two).

paramagnetic behavior following a Curie law (Figure 3). From these data, effective magnetic moments (μ_{eff}) were calculated which are in good agreement with the expected values for the respective ground states (Table 2). This indicates that no magnetic coupling occurs between the Ln^{3+} ions in the framework.

DLS measurements of aqueous suspensions (without any surfactant) showed that they are stable for a considerable time, varying from about 20 min in a strong magnetic field (11.7 T), to more than 2 h without magnetic field applied. The size distributions as obtained by DLS are in agreement with the results of TEM and SEM. This is illustrated for the Ho^{3+}-containing particles in Supporting Information, Figure S1, showing a size distribution between 400 and 1000 nm, with maximum intensity at 615 nm.

The MOF particles remained suspended throughout the NMR measurements and, therefore, it was possible to collect consistent relaxation data. Each lanthanide ion in the particles has one water molecule in its first coordination sphere, leading to significant longitudinal (r_1) and transverse (r_2) relaxivities to be expected for these [Gd(H_2cmp)(H_2O)] particles in aqueous suspensions on the basis of standard inner-sphere relaxation mechanisms operating for small water-soluble complexes.[2,3] However, this theory does not necessarily apply to such particles. In fact, the r_1 values obtained were very low ($r_1 = 1.08 \pm 0.23\ s^{-1}\ mM^{-1}$, 500 MHz, 298 K), which could be due to several factors: inadequate exchange rate between the Gd-coordinated water molecules and the bulk water, leading to a too long residence time of the water molecule at the inner coordination sphere; or hindered diffusion of this water molecule through the framework. By contrast, a high transverse relaxivity ($r_2 = 121.7 \pm 0.3\ s^{-1}\ mM^{-1}$, 500 MHz, 298 K) was observed for the suspensions of these Gd^{3+}-containing particles (Figure 4). These r_1 and r_2 relaxivities are very similar to those reported at 400 MHz (9.4 T) for [Gd_2(bhc)(H_2O)$_6$] (bhc = benzenehexacarboxylate) MOF nanoparticles,[34a] although in that material each Gd^{3+} ion has three water molecules in its inner coordination sphere instead

(36) Barge, A.; Cravotto, G.; Gianolio, E.; Fedeli, F. *Contrast Media Mol. Imaging* **2006**, *1*, 184–188.
(37) Evans, D. F. *J. Chem. Soc.* **1959**, 2003–2005.
(38) Corsi, D. M.; Platas-Iglesias, C.; Bekkum, H.; Peters, J. A. *Magn. Reson. Chem.* **2001**, *39*, 723–726.

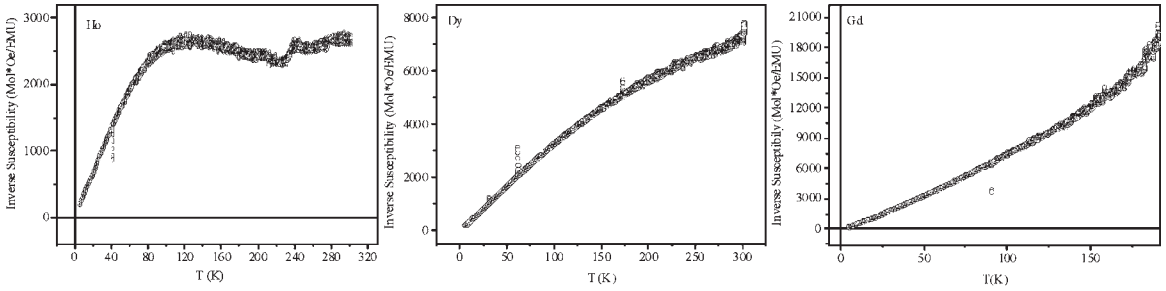

Figure 3. Susceptibility data for [Ln(H_2cmp)(H_2O)] (Ln = Gd, Dy, and Ho). The results are present as the inverse of susceptibility as a function of temperature (K).

Table 1. Parameters Obtained from Analysis of R_2 and R_2* Values of Aqueous Suspensions of [Ln(H_2cmp)(H_2O)] at B = 11.7 T and 298 K[a]

	Ho	Tb	Gd	Nd	Eu	Gd (small)	Gd (large)
$\Delta\omega(r_p)$/MHz[b]	4.45 (0.02)	3.61 (0.03)	2.22 (0.04)	1.24 (0.01)	1.07 (0.01)	7.65 (0.10)	2.89 (0.01)
$\tau_D(r_p)$/ms[b]	2.42 (0.38)	2.32 (0.49)	1.33 (0.42)	0.82 (0.18)	0.67 (0.16)	0.55 (0.20)	1.54 (0.46)
$10^4\, r_{eff}/r_{diff}$[b]	0.75 (0.08)	8.77 (1.39)	3.31 (0.84)	3.38 (0.66)	4.77 (1.08)	1.20 (0.44)	0.67 (0.18)
R_2^{0}[b]	28.4 (4.1)	24.3 (4.4)	30.4 (6.6)	10.3 (0.9)	13.1 (1.0)	62.8 (18.6)	7.0 (2.3)
r_p/μm[c]	2.20 (0.17)	2.16(0.09)	1.67 (0.17)	1.28 (0.13)	1.16 (0.13)	1.05 (0.22)	1.76 (0.30)
r_2*/mM^{-1}.s^{-1}	857.1	677.3	451.3	236.3	217.0	1513.0	556.5

[a] r_2* relaxivities are also shown. [b] From fitting of experimental data with eqs 5 and 6 (Appendix). [c] Calculated from the best-fit values of $\tau_D(r_p)$, and the experimentally determined value of D_0.

Table 2. Magnetic Susceptibility Measurements of [Ln(H_2cmp)(H_2O)] (Ln = Gd, Ho and Dy), at 51 mT

Ln	Curie constant (emuK/gGauss)	effective magnetic moment μ_{eff} (B.M.) (experimental)*	effective magnetic moment μ_{eff} (B.M.) (expected)
Gd	0.74 (0.05)	7.73	7.94
Ho	0.84 (0.05)	10.40	10.65
Dy	1.52 (0.26)	10.20	10.61

* The measurement of magnetization causes an uncertainty of about 1% (mainly by deviations of the model). Since the determination of the mass has an uncertainty of about 0.2 mg, the values can be considered consistent with those expected. Because of the low mass of material in the Gd samples, the inaccuracy was higher in this case, and two measurements at different magnetic fields were performed to determine μ_{eff} independently of the measurement of the mass.

of one found for the system studied here. This confirms that the water proton relaxation in these MOF materials occurs through an outer-sphere mechanism. Higher r_1 values are observed for aqueous suspensions of other MOFs, such as for crystalline [Gd(1,4-bdc)$_{1.5}$(H_2O)$_2$] nanorods (1,4-bdc = benzene-1,4-dicarboxylate) of lengths in the 100−1000 nm range and 40−100 nm diameters, with r_1 and r_2 values of 35.8−20.1 s^{-1} mM^{-1} and 55.6−45.7 s^{-1} mM^{-1}, respectively, and of [Gd(1,2,4-btc)(H_2O)$_3$] nanoplates (1,2,4-btc = benzene-1,2,4-tricarboxylate) of 100 nm in diameter and an average thickness of 35 nm, with r_1 of 13.0 s^{-1} mM^{-1} and r_2 of 29.4 s^{-1} mM^{-1}.[34b] The inverse size dependence of the r_1 and r_2 relaxivities obtained for the nanorods indicates that the Gd^{3+} centers at or near the surface are primarily responsible for their values, since those in the nanomaterial interior may have a decreased water exchange because of hindered diffusion of water molecules through the frame.[15b,34b] A similar situation was reported for the r_1 relaxivities of amorphous nanoparticles of supramolecular coordination polymer networks spontaneously self-assembled from nucleotides, such as 5′-AMP, and Gd^{3+} ions in water.[34c] Surprisingly high relaxivities (r_1 and r_2 up to 105.36 and 129.63 s^{-1} mM^{-1} at 64 MHz, respectively) have been reported for [Gd(1,4-bdc)$_{1.5}$(H_2O)$_2$] nanoparticles surface modified with poly[*N*-(2-hydroxypropyl)methylacrylamide].[34c] This phenomenon has been attributed to the increased water retention by the hydrophilic polymer attached to the surface of these particles.

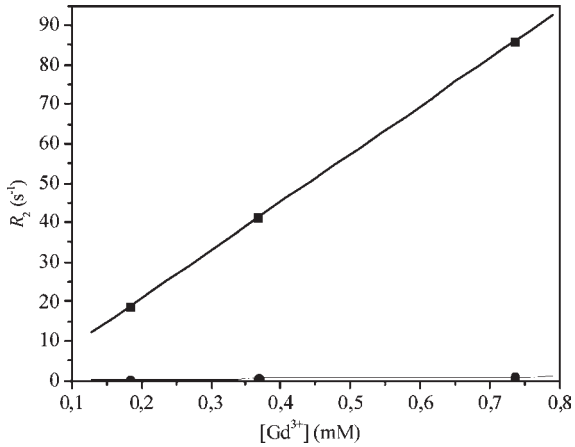

Figure 4. Longitudinal R_1 (●) and transverse R_2 (■) relaxation rates of aqueous suspensions of [Gd(H_2cmp)(H_2O)] as a function of Gd^{3+} content (11.7 T, 298 K).

The water resonances of the aqueous samples of the various [Ln(H_2cmp)(H_2O)] particles showed substantial line broadenings, which can be attributed to the dephasing of the water proton magnetic moments diffusing through the magnetic field gradients in the vicinity of the magnetized particles. The effective transverse relaxivities (r_2*) were obtained from ^{1}H spectral linewidths of the water resonances and the paramagnetic contribution was obtained by subtraction of the r_2* values measured for analogous samples of the diamagnetic [Y(H_2cmp)(H_2O)] (see Table 1). The R_2 values, measured as a function of the time interval between two consecutive 180° pulses (τ_{CP}) in a CPMG pulse sequence, increase with τ_{CP} and reach a limiting value which is, for all paramagnetic lanthanides studied, about 3−5 times lower than the observed r_2* (Figure 5). This behavior is typical for particles for which the transverse relaxivities of aqueous suspensions can be explained by the static dephasing regime

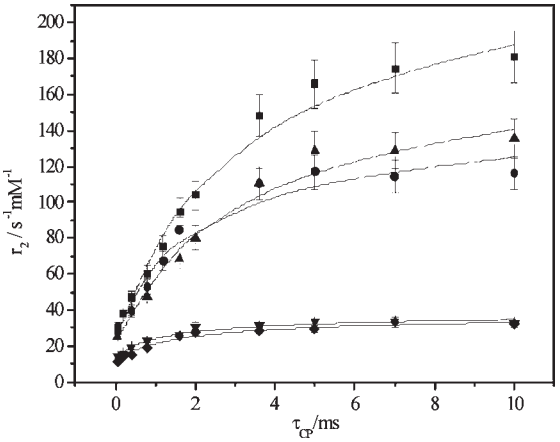

Figure 5. Dependence of r_2 on τ_{CP} for different aqueous suspensions of [Ln(H_2cmp)(H_2O)], at 11.7 T, 298 K ([Ln] = 0.735 mM); Ho (■), Gd (●), Tb (▲), Eu (▼) and Nd (♦).

(SDR) theory,[39−41] in which the diffusion effect is taken into account and where the condition $\tau_D > \Delta\omega(r_p)^{-1}$ holds ($\tau_D = r_p^2/D$, where D is the diffusion coefficient, r_p is the radius of the particle and $\Delta\omega(r_p)$ is the Larmor frequency shift at the particle's surface). The saturation values of r_2 relaxivities are proportional to μ_{eff}^2, where μ_{eff} is the effective magnetic moment of the lanthanide ions (Supporting Information, Figure S2).

The [Ln(H_2cmp)(H_2O)] MOF particles are not spherical; they are thin plates or plate-like aggregates. Therefore, we applied a simplified and qualitative model that previously was used to explain the transverse relaxivities of Ln-AV-9 microparticles.[42] Thus, the particles were approximated with spherical particles with a radius r_p, and it was assumed that the SDR condition, $\tau_D(r_p) \gg 1/\Delta\omega(r_p)$, is fulfilled for these effective spheres. At that regime, the local differences in the nuclear frequencies occur faster than the diffusion phenomena manage to average out the phases of different nuclei and a continuum of proton Larmor frequencies $\Delta\omega_{loc}$ ($\Delta\omega_{loc} = \gamma B_{loc}$). As a consequence, the dependence of R_2 on τ_{CP} comes from the existence of one specific regime, in which the condition $\tau_D(r_p) < 1/\Delta\omega_{loc}$ is valid. Then, when $\tau_{CP} < \tau_D(r_p)$, R_2 increases with τ_{CP}, but when τ_{CP} reaches values higher than $\tau_D(r_p)$, the dephasing is complete and R_2 is no longer dependent on τ_{CP} and becomes constant. In this case, the protons present in the region where this regime (denoted previously as regime A) applies contribute to R_2. However, another possible regime (regime B) is characterized by $\tau_D(r_p) > 1/\Delta\omega_{loc}$. If $\tau_{CP} > 1/\Delta\omega_{loc}$, the situation is similar to that described for regime A and $\tau_{CP} > \tau_D(r_p)$. Protons under this condition are basically lost from the magnetization pool because their dephasing time is shorter than both the diffusion time and the time interval between two refocusing pulses and, consequently, they are not refocused by the π pulses and do not contribute to R_2. If $\tau_{CP} < 1/\Delta\omega_{loc}$ (and $\tau_{CP} < \tau_D(r_p)$), the protons are fully refocused, so they do not contribute to R_2 as well. The whole system was approached as the weighted average of two regions, representing the locations where regime A and B apply. The equations

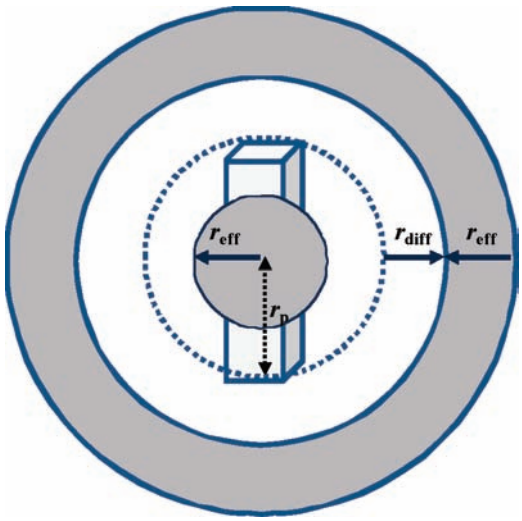

Figure 6. Schematic representation of an approximation of a nonspherical particle to a sphere with radius r_p and the imaginary spheres with radii r_{eff} and r_{diff} (adapted from ref 42).

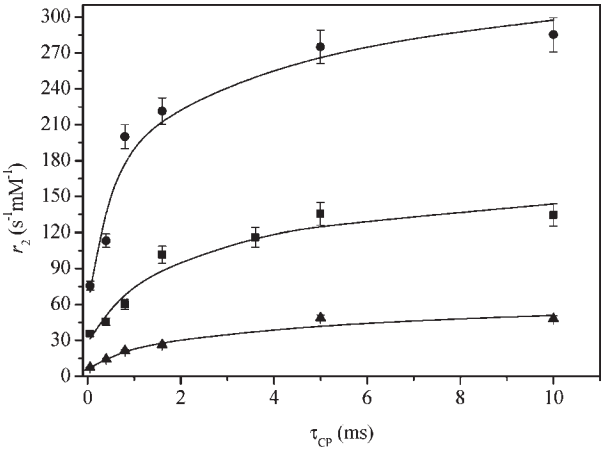

Figure 7. Dependence of r_2 on τ_{CP} for aqueous suspensions of [Gd(H_2cmp)(H_2O)] before and after separation of fractions with different size distributions: not separated (■), smaller (●) and larger particles (▲) at 11.7 T, 298 K.

that describe the transverse relaxivities under these conditions (eqs 5 and 6) are given in the Appendix.

The experimental R_2 and R_2* data for different aqueous suspensions of [Ln(H_2cmp)(H_2O)] particles at B = 11.7 T and 298 K were fitted to eqs 5 and 6 using $\Delta\omega(r_p)$, $\tau_D(r_p)$, r_{eff}/r_{diff}, and R_2^0 as adjustable parameters. As defined previously,[14] r_{eff} is the radius of an imaginary sphere in which protons that are present in this region contribute to R_2 and r_{diff} is another imaginary sphere defined as $r_{diff} = \Delta\omega(r_p)\, r_p^3/D_0$ and which forms the border between protons contributing to R_2 and those not contributing to the transverse relaxation rate (Figure 6). R_2^0 is the contribution due to other relaxation mechanisms, such as the diamagnetic relaxation and a contribution resulting from chemical exchange of protons between the surface of the particles and the bulk water protons. The best-fit parameters are given in Table 1 and curves calculated with these parameters are displayed in Figure 5. The relaxivity fitting results and r_p values are in reasonable agreement with the DLS data, considering the shape of the particles, the assumptions made during the fittings, and mainly the very broad size distribution of these particles.

(39) Brown, R. J. S. *Phys. Rev.* **1961**, *121*, 1379–1382.
(40) Yablonskiy, D. A.; Haacke, E. M. *Magn. Reson. Med.* **1994**, *32*, 749–763.
(41) Gillis, P.; Moiny, F.; Brooks, R. A. *Magn. Reson. Med.* **2002**, *47*, 257–263.
(42) Pereira, G. A.; Norek, M.; Peters, J. A.; Ananias, D.; Rocha, J.; Geraldes, C. F. G. C. *Dalton Trans.* **2008**, 2241–2247.

The best-fit values for the diffusion correlation time (see Table 1) are between 0.6−2.4 ms, which is substantially larger than the values for $1/\Delta\omega(r_p)$ (0.9−2.2 μs), which is consistent with the assumption made above that the SDR regime applies for these particles.[39]

To evaluate the effect of the particle size, the [Gd(H_2cmp)(H_2O)] sample was separated into two fractions of particles (smaller and bigger ones) by means of centrifugation. Relaxivity measurements followed by the theoretical fittings were performed (Figure 7). The particle sizes were estimated by DLS measurements (Supporting Information, Figure S1), showing a narrower size distribution for the smaller particles (with maximum intensity at 400 nm) than for the larger ones (with maximum intensity at 1000 nm). As expected from the SDR model, the smaller particles display larger r_2 values than the larger particles.

Conclusions

[Ln(H_2cmp)(H_2O)] microparticles appear to be very efficient as potential MRI CAs for T_2-weighted imaging, but not efficient for T_1-weighted imaging, despite the presence of one water molecule in the inner-sphere of coordination. The r_2 relaxivity of these MOF particles is similar to that reported for [Gd_2(bch)(H_2O)$_6$] MOF nanoparticles.[34a] The transverse relaxivity effects can be explained well by using a previously described simplified qualitative model[14] considering the SDR adapted for non-spherical and large particles. From the synthetic procedure, we obtained a very broad size distribution of these particles. As expected for the SDR model, the transverse relaxivities increase with decreasing particle size. It should be expected that a maximum relaxivity will be reached at the border between the SDR and the outer sphere (OS) regimes. In the OS regime, the values of r_2 and r_2* are about equal and increase linearly with the value of τ_D.[43]

The r_2 values of [Gd(H_2cmp)(H_2O)] MOF particles are much larger than those measured for xanthan coated Gd_2O_3 nanoparticles[14] or Gd-AV-9 particles,[42] and the r_2* values are similar. However, a direct comparison of these systems is not possible since in those cases xanthan, used as an emulsifier, reduces the r_2 values largely, since the water layer in and close to the adsorbed xanthan is relaxation-silent.[14]

Acknowledgment. We thank Dr. Victor Amaral and Dr. Soma Das (University of Aveiro) for the magnetic susceptibility measurements and data interpretation. This work was supported by the Foundation of Science and Technology (F.C.T.), Portugal (project PTDC/CTM/73243/2006 and Grant SFRH/BPD/35005/2007 to G.A.P.) and FEDER. This work was carried out in the frame of COST Action D38 "Metal-Based systems for Molecular Imaging Applications" and the EU Network of Excellence European Molecular Imaging Laboratory (EMIL, LSHC-2004-503569).

Appendix

The theory of Jensen and Chandra[44] can be applied in our case if we assume that the particles are spherical with radius r_p and they cause weak magnetic inhomogeneities with a radius r_{eff}. Assuming a Gaussian shape of the field correlation function and irregular objects with unrestricted diffusion, eq 1 is obtained:

$$R_2 = R_2^0 + \frac{1}{2}(\Delta\omega^{eff})^2 f^{eff} \tau_D{}^{eff} F(x) \quad (1)$$

where

$$F(x) = \frac{1}{\sqrt{\pi}} \int_0^\infty dy \frac{e^{-y}}{\sqrt{y}} \left[1 - \frac{1}{xy}\tanh(xy)\right]$$

and

$$x = \frac{4\tau_{CP}}{\tau_D(r_{eff})}$$

Here, f^{eff} is the volume fraction of the sphere with radius r_{eff}, $R_2{}^0$ and r_{diff} have the same meaning as explained in the text.

To obtain $\Delta\omega^{eff}$, $\tau_D{}^{eff}$, and f^{eff}, the parameters $\Delta\omega(r_p)$, $\tau_D(r_p)$, and $f(r_p)$ are scaled as follows:

$$\Delta\omega^{eff} = \Delta\omega(r_p)\left(\frac{r_{eff}}{r_{diff}}\right)^3 \quad (2)$$

$$\tau_D{}^{eff} = \tau_D(r_p)\left(\frac{r_{diff}}{r_{eff}}\right)^2 \left(\frac{D}{D_0}\right) \quad (3)$$

$$f^{eff} = f(r_p)\left(\frac{r_{diff}}{r_{eff}}\right)^3 \quad (4)$$

D_0 corresponds to the majority of water protons at some distance from the surface of the particle, while D corresponds to the protons in the closest vicinity of the particles, where the conditions are such that the diffusion may be restricted. R_2* is approximated with the SDR equation for spherical particles (eq 5), where the diffusion correlation time is completely neglected.[40−42,45,46]

$$R_2^* = \frac{1}{T_2^*} = R_2^0 + 2\pi\sqrt{3} f(r_p)\,\Delta\omega(r_p)/9 \quad (5)$$

where $f(r_p)$ is a volume fraction occupied by the particles. Substitution of eqs 2−4 into eq 1, gives eq 6:

$$R_2 = R_2^0 + \frac{1}{2}\Delta\omega(r_p)^2 f(r_p)\,\tau_D(r_p)\left(\frac{r_{eff}}{r_{diff}}\right)\left(\frac{D}{D_0}\right)F(x) \quad (6)$$

For long τ_{CP} ($\tau_{CP} > \tau_D(r_p)$), eq 6 simplifies to

$$R_2 = R_2^0 + \frac{1}{2}\Delta\omega(r_p)^2 f(r_p)\,\tau_D(r_p)\left(\frac{r_{eff}}{r_{diff}}\right)\left(\frac{D}{D_0}\right) \quad (7)$$

Substitution of r_{diff} into eq 6 gives:

$$R_2 = R_2^0 + \frac{1}{2}\Delta\omega(r_p) f(r_p)\left(\frac{r_{eff}}{r_p}\right) \quad (8)$$

Supporting Information Available: DLS of (A) [Ho(H_2cmp)(H_2O)] aqueous suspension as a function of time; (B) [Gd(H_2cmp)(H_2O)] aqueous suspension before and after mechanical separation (Figure S1); Plot of water r_2 versus $\mu_{eff}{}^2$ of the Ln^{3+} ions for different aqueous suspensions of [Ln(H_2cmp)(H_2O)] particles at B = 11.7 T (500 MHz) and 298 K (Figure S2). This material is available free of charge via the Internet at http://pubs.acs.org.

(43) Brooks, R. A.; Moiny, F.; Gillis, P. *Magn. Reson. Med.* **2001**, *45*, 1014–1020.
(44) Jensen, J. H.; Chandra, R. *Magn. Reson. Med.* **2000**, *44*, 144–156.
(45) Muller, R. N.; Gillis, P.; Moiny, F.; Roch, A. *Magn. Reson. Med.* **1991**, *22*, 178–182.
(46) Weisskoff, R. M.; Zuo, C. S.; Boxerman, J. L.; Rosen, B. R. *Magn. Reson. Med.* **1994**, *31*, 601–610.